Open Water results comparison for three propellers with transition model, applying crossflow effect, and its comparison with experimental results *

Moran-Guerrero Amadeo[1], Gonzalez-Adalid Juan[2], Perez-Sobrino Mariano[2], Gonzalez-Gutierrez Leo[1]

[1]Canal de Ensayos Hidrodinámicos de Navales (CEHINAV), Universidad Politécnica de Madrid, Madrid, España
[2]SISTEMAR, Madrid, España

ABSTRACT

At model scale, conventional turbulence models assume turbulent regime all over the propeller's blade surface and consequently not enough accurate results are obtained when laminar regions before transition are not included in the simulation. For this reason, modern CFD, incorporate transition models that quantitatively improve the accuracy of the results being now very comparable to experimental results.

One of the most popular transition models is the well known $\gamma - Re_{\Theta}$. Last year, this model was extended to include crossflow effects by Langtry et al. [2015], without any violation of the (Local Correlation-based Transition Model) LCTM approach. This inclusion overcomes one of the weakness of this transition model, where the correlation method previously implemented was basically applied to bypass and natural Tollmien-Schlichting(TS) transition.

The new $\gamma - Re_{\Theta}$ implementation, where crossflow effects are taken into account, has been compared to the conventional $\gamma - Re_{\Theta}$ transition model and the fully turbulent $k - \omega - SST$ turbulence model for a conventional propeller, a tip rake propeller and a CLT propeller. The study includes a wide range of advance ratios and a complete mesh convergence process that has been carried out in order to minimize meshing errors.

Keywords

transition, propellers, scaling, meshing, CLT propellers

1 INTRODUCTION

Numerical simulations are becoming more and more important nowadays to investigate complex fluid phenomena. This powerful tool, permits designers to go deeper in the details of the design process.

At model-scale Reynolds number and sometimes at full scale propeller where propeller is not big enough or in a twin screw ship, the flow over the propeller can be characterized by three different flow regimes, laminar, transitional and turbulent. From the analysis derived of several paint tests performed in towing tanks, the aspect of the paint over the propeller confirms different regions on the blade where laminar and turbulent flows can be distinguished. Several examples where transition is appreciated on a propeller blade are discussed in Sánchez-Caja et al. [2014], Bha [2016]. With the conventional turbulence models such as $k - \omega$ or $k - \epsilon$, fully turbulent boundary layers are assumed and consequently the friction forces all over the blade are typically over predicted. For this reason, in order to have an accurate prediction at model-scale with CFD codes, it is necessary to take into account these transition effects in the turbulence modelization. In our calculations, transition effects are quantified by the $\gamma - Re_{\theta}$ transition model. This implementation has demonstrated capacity to deal with flat plates, 2D airfoils, 3D multi-element airfoils, and was recently applied to some propellers Bhattacharyya et al. [2015]. The main objective of this study is to observe the differences between different transition models at model-scale calculations.

In 2015, the $\gamma - Re_{\theta}$ transition model was extended to capture crossflow effects by Langtry et al. [2015], without any violation of the LCTM approach. The authors consider the importance of adding the new crossflow correlation when propellers are calculated at model scale due to the twist in the propeller boundary layer, see figure (2 and 1). An evident similarity can be found when compared with the scheme of a normal 3D boundary-layer in a swept-wing.

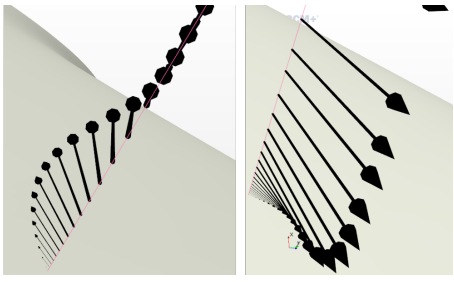

Figure 1: Boundary layer extracted from CFD computation of the VP1304 propeller of the ITTC benchmark.

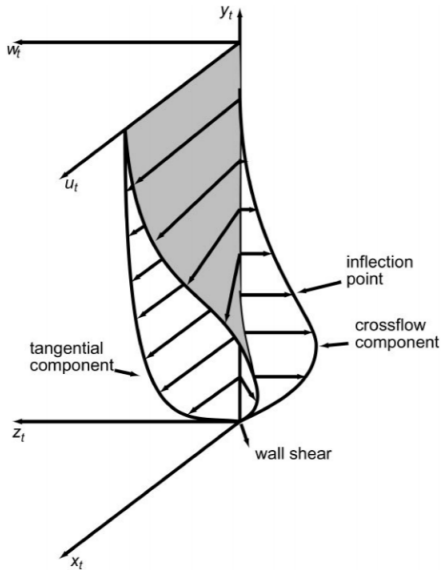

Figure 2: Boundary layer scheme where crossflow effects are included from Saric et al.

This paper is distributed as follows: first, a description of the numerical method applied in the calculation, followed by a description of the problem, the mesh convergence process carried out and the results for all propellers studied. At the end of the paper a brief discussion of the results and the conclusions are included.

2 NUMERICAL METHOD

To carry out this study the RANS solver of Star-CCM+ software was used. This software has been used in numerous works in different parts of hydrodynamics and in particular in propellers computations. Three different approaches to model the flow in the boundary layer are compared in this paper, the well known $k\omega - SST$ and two versions of the $\gamma - Re_\theta$ correlation-based transition model, the original one for TS and bypass transition and an extended version capable to model cross-flow effects.

The boundary conditions for these cases are the ones usually found in the literature. The propeller blades are modeled as rotating non-slip surfaces with the velocity field matching the propeller rotational speed. A uniform flow condition is applied to the inlet and peripheral surfaces. At the outlet, the streamwise gradients of the flow variables as well as the pressure difference are set to zero. For uniform flow computations, only one blade has been used due to the periodicity of the propeller's geometry.

2.1 Transition

The first explanation and details of the $\gamma - Re_\theta$ correlation-based transition model were published by Menter et al. [2004] and Menter et al. [2006] but the full formulation of this model with the experimental correlation was published by Langtry and Menter [2009]. A few months later Malan et al. [2009] published a calibration of the model for commercial CFD codes. Recently this model has been extended in order to be able to capture stationary crossflow effects by Muller and Herbst [2014] and Langtry et al. [2015]. One of the purposes of this study is to compare this modification with the original model and see how it affects the propeller performance at model scale.

2.1.1 Brief description of the $\gamma - Re_\Theta$ transition model

The $\gamma - Re_\Theta$ transition model only computes local variables and gradients. This model solves two additional transport equations, one for the intermittency (γ) and other for the transition onset momentum-thickness Reynolds number ($\overline{Re}_{\Theta t}$).

The transport equation for the intermittency is coupled with the turbulence model, and depending on the intermittency values turns on the turbulence model or maintains the laminar regime. In our case the $k\omega - SST$ was used as turbulence model, but theoretically any other turbulence model could be coupled. The transport equation for $\overline{Re}_{\Theta t}$ is an essential part of the model and works as an interface between the experimental correlation and the intermittency equation.

The general equations for the two transported scalars regarding transition are:

$$\frac{D\rho\gamma}{Dt} = P_\gamma - E_\gamma + \nabla \cdot [(\mu + \frac{\mu_t}{\sigma_f})\nabla\gamma] \quad (1)$$

$$\frac{D\rho\overline{Re_{\theta t}}}{Dt} = P_\theta t + \nabla \cdot [\sigma_{\theta t}(\mu + \mu_t)\nabla\overline{Re_{\theta t}}] \quad (2)$$

where ρ and μ are the fluid density and viscosity, μ_t is the turbulent viscosity, P_γ and $P_\theta t$ represent the production terms, E_γ represents the intermittency destruction term. The factors σ_f and $\sigma_{\theta t}$ are constants of the model.

A complete description of the model and its formulation with the production and destruction terms and constants of the model can be found at Malan et al. [2009].

The addition in order to capture cross-flow effects is based on considering the streamwise vorticity ($\Omega_{Streamwise}$) as an indicator of the local crossflow strength in the boundary layer.

$$H_{Crossflow} = \frac{y\Omega_{Streamwise}}{U} \quad (3)$$

where y is the wall normal distance and U is the total velocity magnitude.

The new empirical correlation for capture cross-flow effect ($Re_{\Theta tSCF}$) is function of the $H_{Crossflow}$ and the surface roughness (h). The full description of the new correlation, including production, destruction terms and constant can

be found at Langtry et al. [2015].

3 CASES OF STUDY AND SET-UP

3.1 Meshing strategy.

The computational domain has been designed taking into account the geometrical periodicity of the propeller in the azimuthal direction and the fact that the inflow velocity profile is uniform. The diameter of the propeller D will be used as the characteristic length for the definition of the computational domain. The cylindrical sector has $9D$ length and radius of $10D$, inside of which the propeller will be placed at $3D$ behind the inflow boundary and $6D$ ahead of the outflow boundary.

For the meshing strategy, different meshing subdomains were used. The mesh size of these domains is refereed to the 'base size' h^s, used as one of the main parameters in the mesh convergence process. The objective is performing a mesh refinement in all the subdomains in the same proportion, that is what we call 'global remeshing'.

The second parameter in the mesh convergence process is the number of prism layers in the boundary layer, N_{Layers}. Typically, values for this study are between five and thirty, see fig(3). The total thickness of the prism layer, δ_t has been kept constant for all simulations in a percentage of the boundary layer thickness. Wall normal thickness of the wall prism layer, δ_0 is set to the value that permits $y^+ < 1$ all around the blade. This last condition $y^+ < 1$ has been found necessary to obtain a time converged simulation when transition model is used.

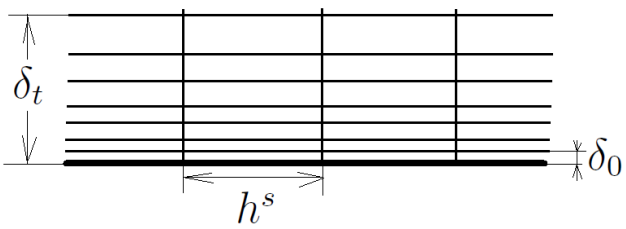

Figure 3: Scheme of the boundary layer mesh parameters.

We perform a complete convergence process increasing the number of layers N_{layers} in the prism layer. The output of this study is monitored during the mesh convergence process of the propeller and determines which number is the critical value of prism layers to be used.

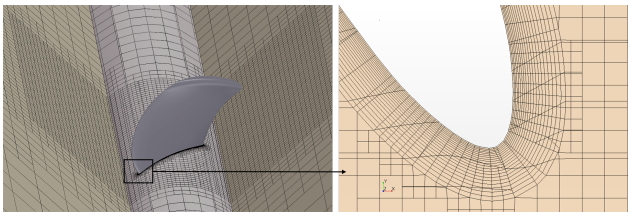

Figure 4: Mesh view close to the propeller(left) and detailed view of the mesh in the leading edge proximities (right).

3.2 Open Water Propellers Study at model scale.

In the current study, three geometries are considered: the two ITTC benchmark propellers test cases, conventional (VP1304) and tip-raked (P1727) geometries and the new generation of (Contracted Loaded Tip) CLT propeller (Gonzalez-Adalid et al. [2016] and Gag [2016]). Although two of them are Controllable Pitch Propellers, this study has been carried out at fixed pitch angle.

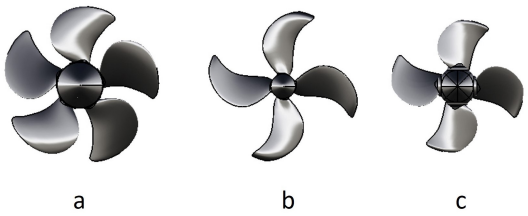

Figure 5: Geometries of the three propellers studied. (a) The VP1304, (b) the P1727 and (c) the new generation of CLT propeller.

All cases have been computed at model scale for different advanced ratios (J). The VP1304 propeller is a five blade conventional propeller while the P1727 and CLT propellers have only four blades. See figure(5).

For all of the propellers studied, experimental results are available at model scale and a comparison with the numerical results is carried out in this paper. In the case of the VP1304 propeller there are also numerical results from different institutions and research groups, see the technical report of SVA. The main geometric characteristics of the propellers are in table(1).

To avoid mesh rotation and re-meshing at each time step, Navier-Stokes equations are solved in a rotation reference frame where inertial forces are included. The propeller is fixed in the computational domain and Moving Reference Frame equations are used.

The range of the advance coefficients studied in this paper is different for each propeller due to different operating point and condition in each propeller. A summary of the

		VP1304	P1727	CLT
Diameter [mm]	D	250.00	238.64	208.00
Pitch at 0.75R [mm]	$P_{0.75}$	407.38	192.01	242.53
Chord at 0.75R [mm]	$Cr_{0.75}$	106.35	55.61	71.14
Thickness at 0.75R [mm]	$Th_{0.75}$	3.79	2.93	2.63
Area Ratio	Ae/Ao	0.78	0.44	0.57
Blades	z	5	4	

Table 1: Main geometric characteristics of the propellers studied.

		PPTC	P1727	CLT
Time asumption	[-]	Steady		
Rotation asumption	[-]	MRF asumption		
Axisymmetric asumption	[-]	Yes		
Diameter [m]	D	0.2500	0.2387	0.2080
Advance Ratio	J	[0.6,0.8,1.0,1.2,1.4]	[0.1,0.3,0.5,0.7,0.9]	[0.6,0.7,0.8,0.9,0.95]
Revolutions [rps]	n	15.0	18.0	15.0
Reynolds at 0.75R	$Re_{0.75}$	$9.009 \cdot 10^5$	$5.0789 \cdot 10^5$	$4.8747 \cdot 10^5$

Table 2: General parameters of the simulations. Reynolds numbers are calculated at J=1.0, J=0.5 and J=0.8 respectively.

conditions studied is presented in table(2).

4 RESULTS

In this section results for the mesh convergence process and the open water calculations are presented. All the parameters for the CFD study and mesh designs are described in section (3). The geometric characteristics of the propellers are quantified in table 1 and the simulation setup for the different propellers in table 2.

4.1 Mesh Influence on the results

A double convergence process has been carried out in this work. Results are presented in terms of the dimensionless thrust K_t and torque $10K_q$. As explained in section(3), the double mesh convergence process is based on two parameters as an indicator of the convergence, in this case the 'base size' and number of layers in the prims layer, N_{Layers}.

Results for the well known VP1304 of the ITTC Benchmark Test Case in terms of dimensionless thrust and torque coefficients are presented in figure(6) for the open water test calculations. Figure(6) shows both convergence processes, first, a pseudo convergence increasing the global base size for a constant number of layers in the boundary layer region, and second, a pseudo convergence process obtained when the number of prisms layers is increased. The results of this bi-parametric process, makes the converged value more trustable than other simpler mesh convergence processes. An additional advantage when this kind of studies is performed is saving computational resources when observing how mesh parameters affect the final converged result. In figure(6), the dotted grey lines represent the convergence process when the global mesh size is fixed and the number of prisms layers is increased. It should be remarked that the number of layers in the boundary layer area seems to be more relevant during the mesh design than the global mesh size in terms of mesh convergence. Consequently we could say that meshes with more than 20 prism layers will have an accurate approximation to the converged final values of K_t and $10K_q$ even when the total number of cells is less just a third of the finest mesh.

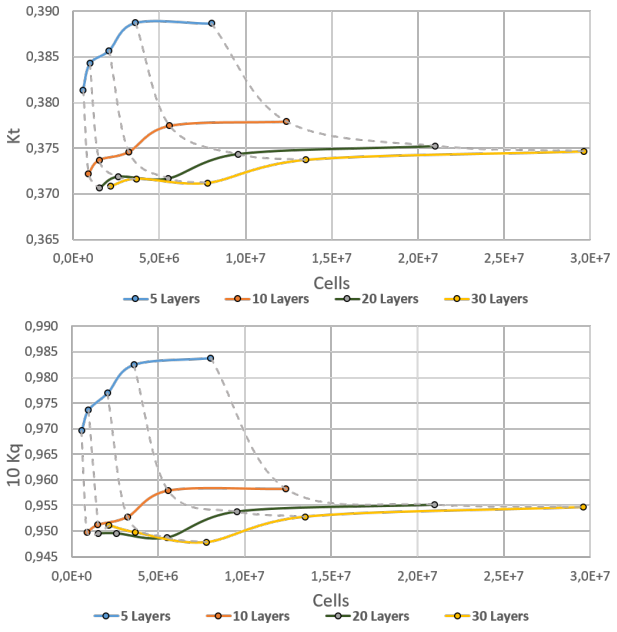

Figure 6: Mesh convergence process for PPTC propeller based on the K_t and $10K_q$ non-dimensional parameters for different number of total cells and prisms layers. Dotted grey lines represent the convergence process when the global mesh size is fixed and the number of prisms layers is increased.

With this methodology, the computational errors due to the mesh are minimized and the final solution is numerically

consistent. The same convergence methodology has been followed for the rest of the propellers, but results are not not shown due to the limited extension of the paper.

4.2 Open Water

4.2.1 VP1304 conventional Propeller

In the next section open water test calculation results of the VP1304 propeller are presented. Experimental measurements in the SVA Towing Tank are available for comparison with computational results, due to the fact that this propeller was selected by the ITTC as a benchmark case. The range of advance coefficients studied are between $J = 0.6$ and $J = 1.4$ both included. In fig(7) we can observe the efficiency open water curve for different methods for the transition and turbulence modeling. It is possible to observe in table(3) the quantitative differences between each method compared to the experimental results obtained from the ITTC-Benchmark. Three different cases were studied, in the first, a fully turbulent case modeled by the $K\omega - SST$ model is used, in the second case a $\gamma Re\Theta$ transition model was added to the computation, and finally in the third case where the crossflow transition is modeled with the transition model. In the last two cases, the errors compared to the experimental values $\Delta\eta_0$ are below two and three per cent and for the fully turbulent case the errors are over ten per cent in the worst case. It is important to remark that when the cross flow correlation is added to the $\gamma Re\Theta$ transition model it improves the results in terms of efficiency η_0 for all advance ratios, leaving it below two percent in the worst case. We can conclude that the improvement obtained when the crossflow term is added to the computational model is remarkable and in good agreement with experimental values. Fig(8) presents the differences in K_t values respect to the experimental results for different advance coefficients. For all the models thrust is overestimated but results shows better agreement with transition models.

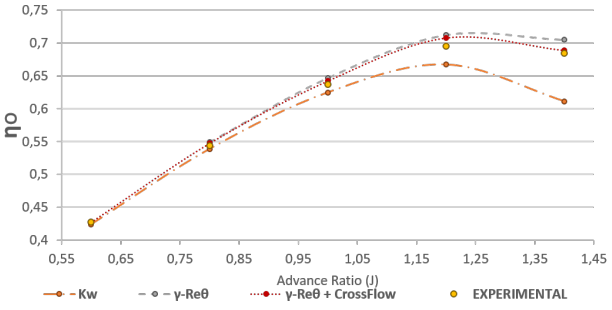

Figure 7: Efficiency values for the open water results for the VP1304 ITTC benchmark propeller.

$\Delta_\eta[\%]$			
J	$Kw - SST$	γRe_Θ	$\gamma Re_\Theta + CF$
0.6	-0.72	0.91	0.02
0.8	-0.98	0.91	0.60
1.0	-1.88	1.59	0.90
1.2	-4.10	2.47	1.88
1.4	-10.70	2.95	0.64

Table 3: Differences on the efficiency values respect to the experimental values for the VP1304 ITTC benchmark propeller.

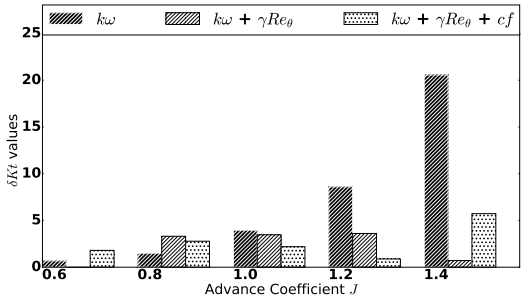

Figure 8: Differences in dimensionless thrust coefficient respect to the experimental values for the VP1304 propeller.

Fig(9) shows the streamlines over suction and pressure side for the three different models studied. The assumption of fully turbulent flow does not show the typical centrifugal component of the streamlines that can be appreciated only when a transition model is included. When the γRe_Θ model is added to the simulation a larger centrifugal component appears in the laminar area on both the suction and pressure sides, while growing transition instabilities that affect the streamlines at large radius near the trailing edge are also appreciated.

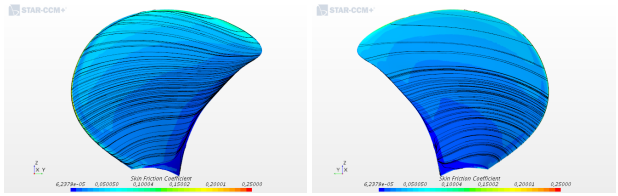

(a) $k\omega$

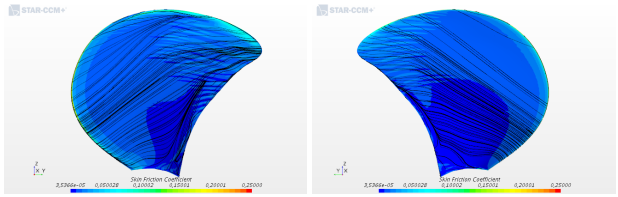

(b) $k\omega + \gamma Re_{\Theta}$

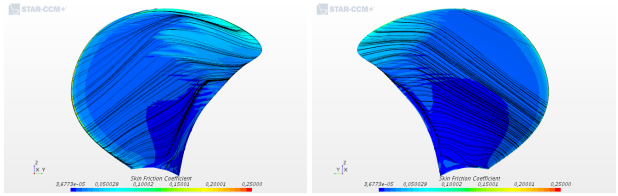

(c) $k\omega + \gamma Re_{\Theta} + CF$

Figure 9: Skin friction contour plot and streamlines representation over the suction(left) and pressure(right) sides for the VP1304 ITTC Benchmark propeller at $J = 1.2$.

If a cross flow term completes the model, higher skin friction coefficients are visualized in the transition area, and consequently the direction of the streamlines changes more abruptly when the transition phenomenon starts.

4.2.2 P1727 Tip-Rake Propeller

In this section results of the non-conventional P1727 Tip-Rake propeller are presented. Analogously to the former VP1304 propeller, the P1727 Tip-Rake propeller was selected by the ITTC as a benchmark case for non convectional propellers. The experimental measurements performed in the SVA Towing Tank are also available for comparison with computational results. The range of advance coefficients studied is between $J = 0.1$ and $J = 0.9$ both included.

In fig(10) we can appreciate the open water curve. Although for $J < 0.5$ the presence of transition models is not very relevant, important differences can be observed for $J > 0.5$ where the γRe_{Θ} with and without transition model approximate the experimental values very accurately with the only exception of $J = 0.9$ which is out of the operative range. In table(4) a relative comparison between each method and the experimental values obtained from the SVA model basin is presented. We can observe that when transition models are used, the differences with the experimental values are always below 2% for all the range of advance coefficients. A comparison with the experimental dimensionless thrust is presented in fig(11) for a range of advance coefficients close to the design point of the propeller. Transition models improve the results in terms of thrust and not only in terms of the global efficiency of the propeller.

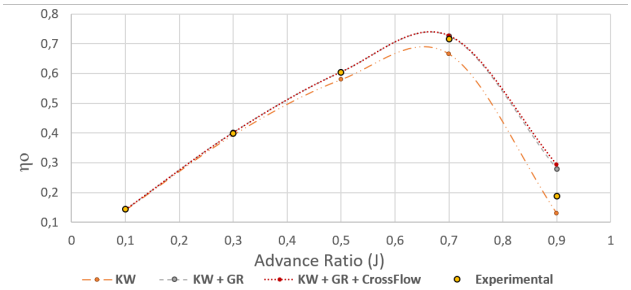

Figure 10: Efficiency values for the open water results for the P1727 ITTC benchmark propeller.

$\Delta_{\eta}[\%]$			
J	$Kw - SST$	γRe_{Θ}	$\gamma Re_{\Theta} + CF$
0.1	-1.43	-0.38	-0.58
0.3	-1.25	+0.96	+0.70
0.5	-3.89	+0.37	+0.36
0.7	-6.92	+1.50	+1.71
0.9	-31.12	+47.92	+55.53

Table 4: Differences on the efficiency values respect to the experimental values for P1727 ITTC benchmark propeller.

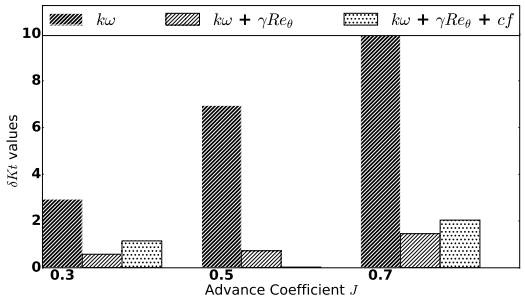

Figure 11: Differences in dimensionless thrust coefficient respect to the experimental values for the P1727 propeller.

Fig(12) shows the streamlines and the skin friction coefficients over suction and pressure sides for the three methods studied. As before, when fully turbulent flow is assumed, the centrifugal component of the streamlines is not very intense and the streamlines follow a radial direction. When the transition models are included, the slope of the streamlines changes noticeably due to the centrifugal component. This could be explained in terms of the ease to rotate the streamlines in the laminar region where the skin friction coefficients are lower, compared to the turbulent areas with higher friction. Near the trailing edge an accumulation of streamlines following the radial direction is appreciated for both transition models. When the crossflow term is added to the simulation, higher skin friction coefficients are ap-

preciated close to the trailing edge.

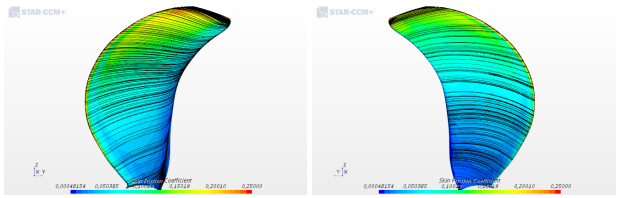

(a) $k\omega$

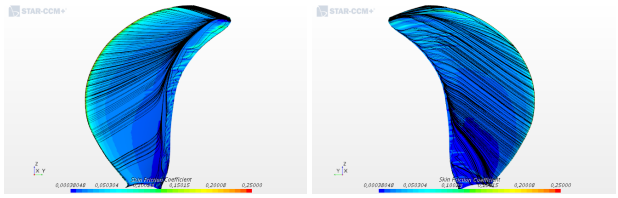

(b) $k\omega + \gamma Re_{\Theta}$

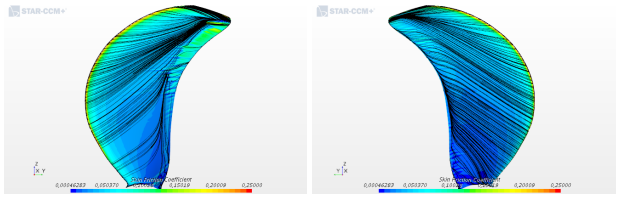

(c) $k\omega + \gamma Re_{\Theta} + CF$

Figure 12: Skin friction contour plot and streamlines representation over the suction (left) and pressure sides (right) of the P1727 ITTC benchmark propeller. J=0.5

4.2.3 New generation of CLT® Propeller

In this section results of the new generation of CLT®propeller are presented. This propeller was experimentally tested in 2016 in the CEHIPAR towing tank facilities. The advance coefficients studied are between -25% and +15% of the design point $J \approx 0.8$.

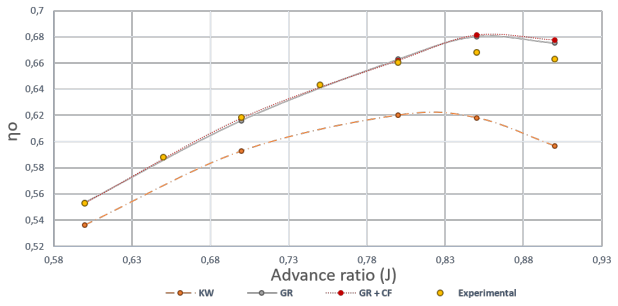

Figure 13: Efficiency values for the open water results for the CLT propeller.

In fig(13) we can see the efficiency open water curve for different turbulence models with and without transition modeling. The use of transition models show good agreement when compared to experiments, and only the two highest advance coefficients show small differences. In order to quantify these differences, table(5) shows a relative comparison between each method and the experimental results obtained from the CEHIPAR model basin. According to table(5), the transition models clearly better approximate the efficiency of the propeller, leaving it almost below two percent. Fig(14) presents the differences in K_t values respect to the experimental results for different advance coefficients. For all the models thrust is underestimated but results shows better agreement with transition models.

$\Delta_\eta[\%]$			
J	$Kw - SST$	γRe_{Θ}	$\gamma Re_{\Theta} + CF$
0.60	-3.0	0.0	0.0
0.70	-4.2	-0.4	-0.1
0.80	-6.1	0.4	0.2
0.85	-7.5	1.8	2.0
0.90	-10.0	1.9	2.2

Table 5: Differences on the efficiency values respect to the experimental values for the new generation of CLT propeller.

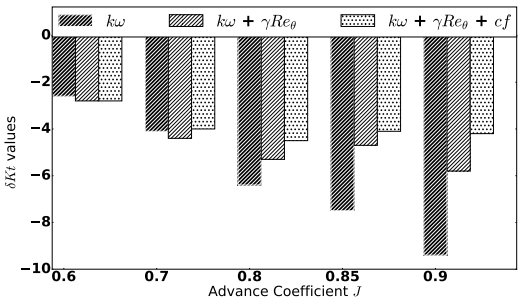

Figure 14: Differences in dimensionless thrust coefficient respect to the experimental values for the CLT propeller.

In order to present a more complete description of the transition that takes place on the CLT propeller, Fig(15) show the streamlines over suction and pressure sides and a contour plot of the skin friction coefficient. As before, three methodologies are used to simulate the turbulent and transition phenomena. As in the other two propellers, when a fully turbulent flow is assumed over the propeller's blade, the centrifugal component barely affects the slope of the streamlines as can be observed in the rest of the images where the transition model is included. Although the images for the γRe_{Θ} with and without crossflow modelization seem to be very similar, small differences can be found and transition occurs for slightly smaller radius when crossflow is modeled in the simulation.

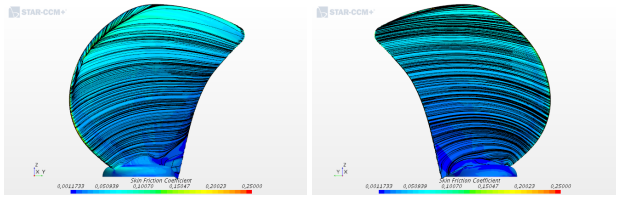

(a) $k\omega$

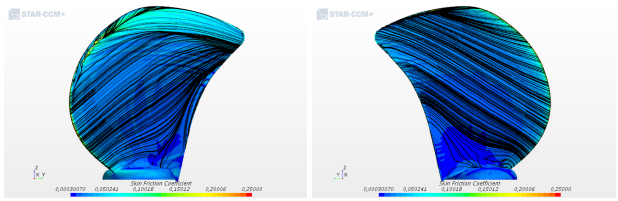

(b) $k\omega + \gamma Re_\Theta$

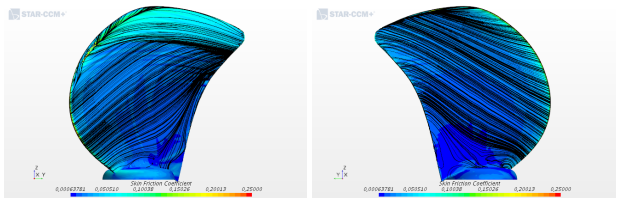

(c) $k\omega + \gamma Re_\Theta + CF$

Figure 15: Skin friction contour plot and streamlines representation over the suction (left) and pressure (right) sides of the new generation of CLT propeller at J=0.8.

5 CONCLUSIONS

In this paper, a complete study of the open water test for three different propellers in terms of mesh and turbulent transition modeling has been carried out.

Regarding the mesh convergence study, the main conclusion is that if the condition of $y^+ < 1$ is assumed all over the blade, a minimum number $N_{layers} \sim 20$ of prism layers should be used in order to have consistent global propeller results at model scale. Nevertheless, a pseudo convergence process decreasing the global mesh size is also obtained when the number of prism layers is fixed.

In terms of turbulent transition modeling, we conclude that the new implemented $Kw - \gamma Re_\Theta$ designed to model the cross-flow transition mechanisms, improves the results in most of the cases. However, the largest differences are found in the VP1304 propeller characterized by the largest Reynolds number. Further analysis should be done to study this phenomenon but this result confirms the importance of the crossflow transition mechanism in propellers at model scale which appears in open water tests and can be also observed in CFD simulations such as in figure(2).

A general trend observed, is that the CFD results show bigger differences compared to experiments when advance coefficients are larger than the operating points.

ACKNOWLEDGMENTS

Part of this work has been made during the framework of the COINCIDENTE R&D project of the Spanish Ministery of Defence. Authors wish to thank the partners in the project and to SVA towing tank.

REFERENCES

Open water tests with the model propeller vp1304. Technical report. URL `http://www.sva-potsdam.de/wp-content/uploads/2016/04/SVA_report_3752.pdf`.

Scale effects on open water characteristics of a controllable pitch propeller working within different duct designs. *Ocean Engineering*, 112:226 – 242, 2016. ISSN 0029-8018.

Design and analysis of a new generation of {CLT} propellers. *Applied Ocean Research*, 59:424 – 450, 2016. ISSN 0141-1187.

A. Bhattacharyya, J.C. Neitzel, S. Steen, M. Abdel-Maksoud, and V. Krasilnikov. Influence of flow transition on open and ducted propeller characteristics. In *Fourth International Symposium on Marine Propulsors, SMP*, 2015.

J. Gonzalez-Adalid, M. Perez-Sobrino, A. Moran-Guerrero, L.M. Gonzalez-Gutierrez, J.M. Riola Rodríguez, J.J. Diaz-Hernandez, R. Quereda-Laviña, and C. Soriano-Gomez. New generation of clt®propellers. In *Maritime Technology and Engineering 3, MARTECH*, 2016.

R.B. Langtry and F.R. Menter. Correlation-Based Transition modelling for Unstructured Parallelized Computational Fluid Dynamics Codes. *AIAA*, 47:2894–2906, June 2009.

R.B. Langtry, K. Sengupta, D.T. Yeh, and A.J. Dorgan. Extending the $\Gamma - Re_\Theta$ Local Correlation based Transition Model for Crossflow Effects. *AIAA*, 47, June 2015.

P. Malan, K. Suluksna, and E. Juntasaro. Calibrating the $\Gamma - Re_\Theta$ transition model for commercial CFD. *AIAA*, 2009.

F.R. Menter, R.B. Langtry, S.R. Likki, Y.B. Suzen, P.G. Huang, and S. Volker. A Correlation-based Transition Model Using Local Variables Part 1- Model Formulation. *ASME*, June 2004.

F.R. Menter, R.B. Langtry, and S. Volker. Transition modelling for general purpose CFD codes. *Flow, Turbulence and Combustion*, 77:277–303, June 2006.

C. Muller and F. Herbst. Modelling of crossflow-induced transition based on local variables. In *11th World Congress on Computational Mechanics, WCCM XI*, 2014.

A. Sánchez-Caja, J. González-Adalid, M. Pérez-Sobrino, and T. Sipil. Scale effects on tip loaded propeller performance using a ranse solver. *Ocean Enginnering*, (88):607–617, 2014.

W.S. Saric, H. L. . Reed, and E. B. White. Stability and transition of three-dimensional boundary layers. *Annual Review Fluid Mechanics*, pages 413–440.